SWIM FM Calibration Report
Issue 1 Revision 0

Martin Wieser
Swedish Institute of Space Physics, IRF, Kiruna, Sweden

January 22, 2010

Document Revision History

Issue	Revision	Date	Remarks
Draft 1	-	26 June 2009	First draft version
Draft 2	-	15 October 2009	Second draft version
1	pre1	10 January 2010	Initial version
1	pre2	14 January 2010	Futaana added comments
1	0	22 January 2010	Initial release

Important note: With release of this version of this document, any earlier version of this document becomes invalid and **must not** be used anymore for data processing.

Contents

Chapter 1

The instrument

1.1 Coordinate systems

Figure 1.1 defines the instrument coordinate system along with the azimuth angle φ and the elevation angle θ used to describe viewing directions.

1.2 Zero-based numbering

Zero based numbering is used throughout this document for pixels, mass bins, energy steps and so on. For different numbering schemes see also Section 3.1.1.

Important note: In early versions of the instrument description and in the TCTM documentation of the DPU a one-based numberig was used for specific cases. **Always check before use!**

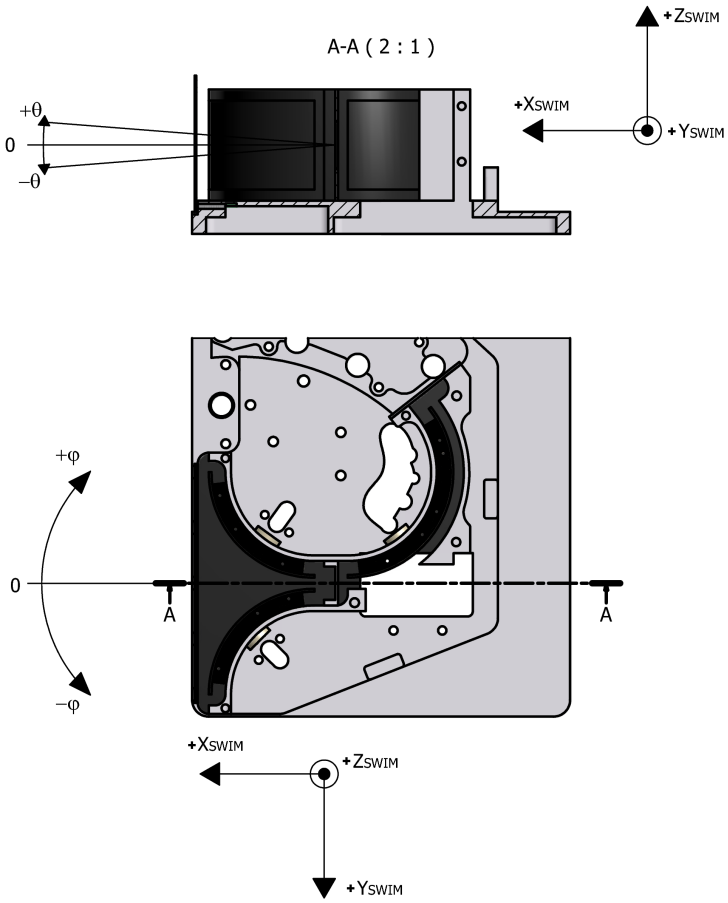

Figure 1.1: SWIM coordinate system

Chapter 2

Electrical interface

2.1 Conversion functions

SWIM contains internally six separately controllable high voltages plus one temperature monitor. Voltages are controlled by references and measured by monitors. There are two sets of conversion functions: a) convert a digital reference value to a predicted voltage, b) convert a digital monitor value to a measured voltage. Both conversions use function of the type

$$y = p\left(ax^2 + bx + c\right) \tag{2.1}$$

where:

- a, b and c are tabulated coefficients,
- x the digital monitor (ADC value; 12 bit) or the digital reference (DAC value; 8 or 12 bit),
- y the corresponding value in physical units and
- p is the polarity of the high voltage.

2.2 Monitors

Conversion coefficients for digital monitor values are given in Table2.1. Note that x is always a positive value. Some high voltages are nevative voltages in the sensor, and some exist in both polarities; the polarity p indicates which case is applicable.

Table 2.1: Coefficients to convert digital monitor values to physical units

Monitor name	a	b	c	Physical unit for y	Polarity p
Main	0.0	1.3567	-6.4155	Volts	+
CEM	2.0e-5	1.2784	0.0	Volts	+
Defl. upper	0.0	1.2053	-4.0	Volts	-
Defl. lower	0.0	1.2085	-4.0	Volts	-
Anyz	0.0	1.1979	-3.2	Volts	-
Cell	7.0e-5	1.1484	8.9559	Volts	-
Temp	0.0	0.101725	-244.08	°C	+

2.3 References

Table 2.2 shows coefficients to convert digital reference values to expected physical units. These values should be used if the monitor readings can not be used for any reason. Note that in order for the predicted voltage to be correct, the expression in parenthesis in Equation 2.1 (prior multiplication with the polarity p) must be positive. If the expression in parenthesis in Equation 2.1 is negative, then the predicted voltages are invalid.

Table 2.2: Coefficients to convert digital references to predicted voltages

Reference name	a	b	c	Physical unit for y	Polarity p
Main	0.0	15.585	221.56	Volts	+/-
CEM	5.0e-4	16.694	-144.48	Volts	+
Defl. upper	-1.0e-6	1.0201	-274.71	Volts	-
Defl. lower	-7.0e-7	1.0191	-272.26	Volts	-
Anyz	-4.0e-6	0.9994	-251.80	Volts	-
Cell	0.0	5.5277	-90.340	Volts	-

Chapter 3

Sensor properties

3.1 Data organization

3.1.1 Numbering and naming schemes

There are various pixel and energy step numbering schemes used for SWIM. All the sensor numbering is zero-based.

DPU numbering: From the point of view of the DPU, SWIM uses 32 energy steps to cover the energy range and 8 deflection steps for angular coverage. Except for some very few datasets during commissioning, all data processed on the DPU used this maximum resolution mode of 8 angular pixels and 32 energy steps. The data matrix produced by the DPU has therefore 8x32 elements. Elements in this matrix are identified by the deflection bin index d and the energy bin index e. This is refered as *DPU numbering.*

Angular ordered numbering: To get angular coverage without gaps, 2 consecutive energy steps have the same energy but slightly different angular viewing directions. This is how SWIM was operated except for very few time during the the commisioning period. This means that SWIM was working in a mode with 16 angular pixels times 16 energy steps. We call this sweeping as *"double angular scan"* hereafter. Data represented in this *double angular scan* mode forms a 16x16 matrix. Elements in this matrix are identified by deflection bin index D and energy bin index E. This is refered as *Angular ordered numbering.* The advantage of angular numbering is that pixels which are neighbors in angular and energy space have numbers which differ by exactly one.

Conversion from *angular ordered numbering* using E, D to *DPU numbering* using e, d is done by

$$e = (E \ll 1) + (D \,\&\, 1) \tag{3.1}$$

$$d = D \gg 1 \tag{3.2}$$

where $\ll$and $\gg$ shows bit shift leftward and rightward, and & bitwise AND operators. Hereafte, Dn and Em notation is used to identify deflection direction n or energy step m (e.g. D1 means the pixel with deflection direction 1 in *angularly ordered numbering*).

Acuisition time ordered numbering: 16 deflection and 16 energy steps $\bar{d}$ and $\bar{e}$ are used. Deflection steps are numbered in the order they are measured.

Named angular pixel: Angular pixels are also given names. The name starts with "CH-" followed by the number 0-7 corresponding to the index d in DPU numbering together with one character 'L' (if e is even) or 'H' (if e is odd).

All pixel numbering schemes are shown in Table 3.1.

In this document angular ordered numbering or pixel names are used except where explicitly noted otherwise.

Table 3.1: Naming of SWIM pixel viewing directions and energy steps for the first (top half) and all following deflection sweeps (bottom half). Columns with bold text indicate the numbering and naming used in this document. Note that two elements in a complete deflection/energy sweep (marked with *) do not actually contain data due to the way SWIM is operated by the DPU.

Angular pixel name	**Angular ordered**		DPU ordered		Acuisition ordered	
	E	**D**	e	d	$\bar{e}$	$\bar{d}$
CH-0L	**0**	**0**	0	0	0	0
CH-0H	**0**	**1**	1	0	0	8
CH-1L	**0**	**2**	0	1	0	1
CH-1H	**0**	**3**	1	1	0	9
CH-2L	**0**	**4**	0	2	0	2
CH-2H	**0**	**5**	1	2	0	10
CH-3L	**0**	**6**	0	3	0	3
CH-3H	**0**	**7**	1	3	0	11
CH-4L	**0**	**8**	0	4	0	4
CH-4H	**0**	**9**	1	4	0	12
CH-5L	**0**	**10**	0	5	0	5
CH-5H	**0**	**11**	1	5	0	13
CH-6L	**0**	**12**	0	6	0	6
CH-6H	**0**	**13**	1	6	0	14
CH-7L	**0**	**14**	0	7	0	7
CH-7H	**0**	**15**	1	7	0	15
CH-0L	**1**	**0**	2	0	1	0
CH-0H	**1**	**1**	3	0	1	8
CH-1L	**1**	**2**	2	1	1	1
...	**...**	**...**	...	...	...	...
...	**...**	**...**	...	...	...	...
CH-6H*	**15**	**13**	31	6	15	14
CH-7L	**15**	**14**	30	7	15	7
CH-7H*	**15**	**15**	31	7	15	15

3.1.2 Accumulation matrix organization in raw data

The data provided by the DPU is organized in 8 deflection x 32 energy bins. Each matrix element is either a set of 5 counters in the case of the accumulation scaling matrix or a set of 32 mass bins for the case of the accumulation matrix. The matrix is addressed using *DPU numbering*. In the raw data the matrix is given as serial data stream organized as follows: *ToDo: insert proper element order here...* , with *EmDn* the matrix element for energy bin m and deflection bin n. Note that counter values are lin-log-encoded, see "SARA_TMTCDOCUMENT_DRAFT_REV5" and "CHA-SARA-DS-0011-I1R1 (SWIM DPU Data Processing Pseudo Code)" for what encoding is used for which counter and how padding is used in the matrix. The last two elements labeled by * in Figure 3.1do not contain scientific data but padded by zero because of the sensor/DPU specification.

3.2 Electrostatic analyzer

3.2.1 Analyzer constant

The electrostaic analyzer is characterized by the linear function

$$E/q = k \cdot V_{ESA} \tag{3.3}$$

where E/q is the particle energy per charge in eV/q, V_{ESA} the voltage on the ESA plate in volts, and k the analyzer constant. k was measured during the ground calibration at 4 different energies and 3 different angles of incidence. For better noise suppression (from what data?) the ESA voltage was calculated using digital reference values with coefficients taken from Table 2.2. Within the given error, the analyzer constant k is independent of energy and angle of incidence (Figure 3.1). The same value for k is valid for start counter and for coincidence events:

$$k = 4.250 \pm 0.005 \tag{3.4}$$

3.2.2 Energy resolution

The width of the energy pass band depends mainly on viewing direction and type of the event data (Figure 3.2). The energy pass band is well approximated by a Gaussian. The energy resolution ($\Delta E/E$), where ΔE and E represents the FWHM values of the energy pass band and the central energy, is given in Figure 3.2. Measurements below 1 keV have larger uncertainities due to worse counting statistics and larger influence of small voltage offset errors. Weighted averages of $\Delta E/E$ for the energy range 100 eV – 3000 eV are given in Table 3.2.

Table 3.2: Weighted average energy resolution $\Delta E/E$ for 100 eV – 3000 eV

Azimuth angle φ [°]	-40	0	+40
Start counter	0.0702±0.001	0.0822±0.001	0.0726±0.001
Coincidence counter	0.0735±0.004	0.0845±0.004	0.0765±0.004

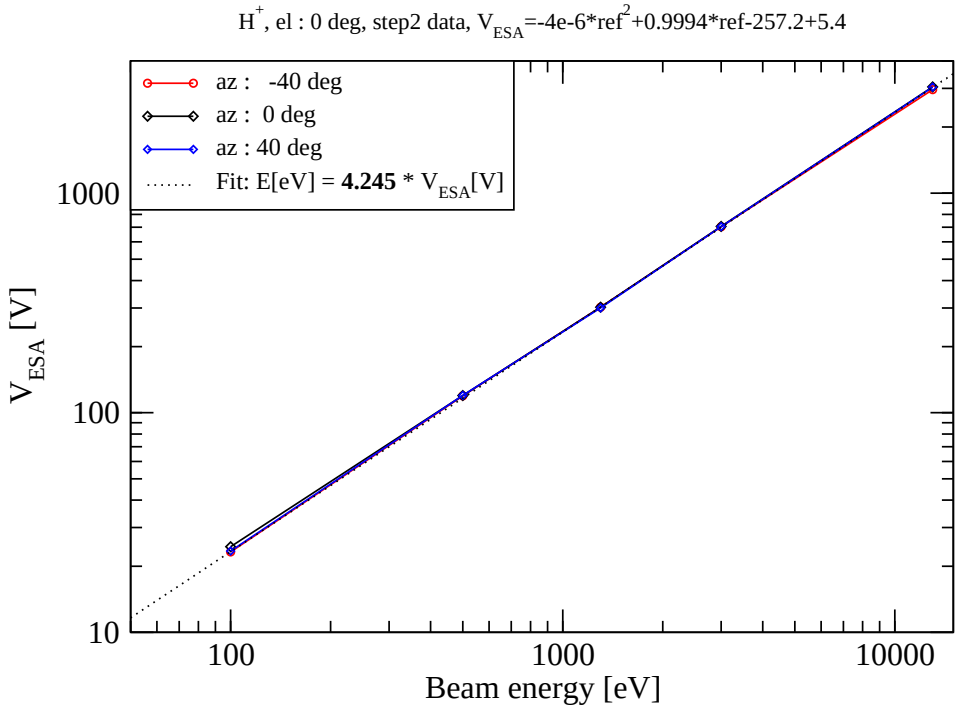

Figure 3.1: Analyzer constant

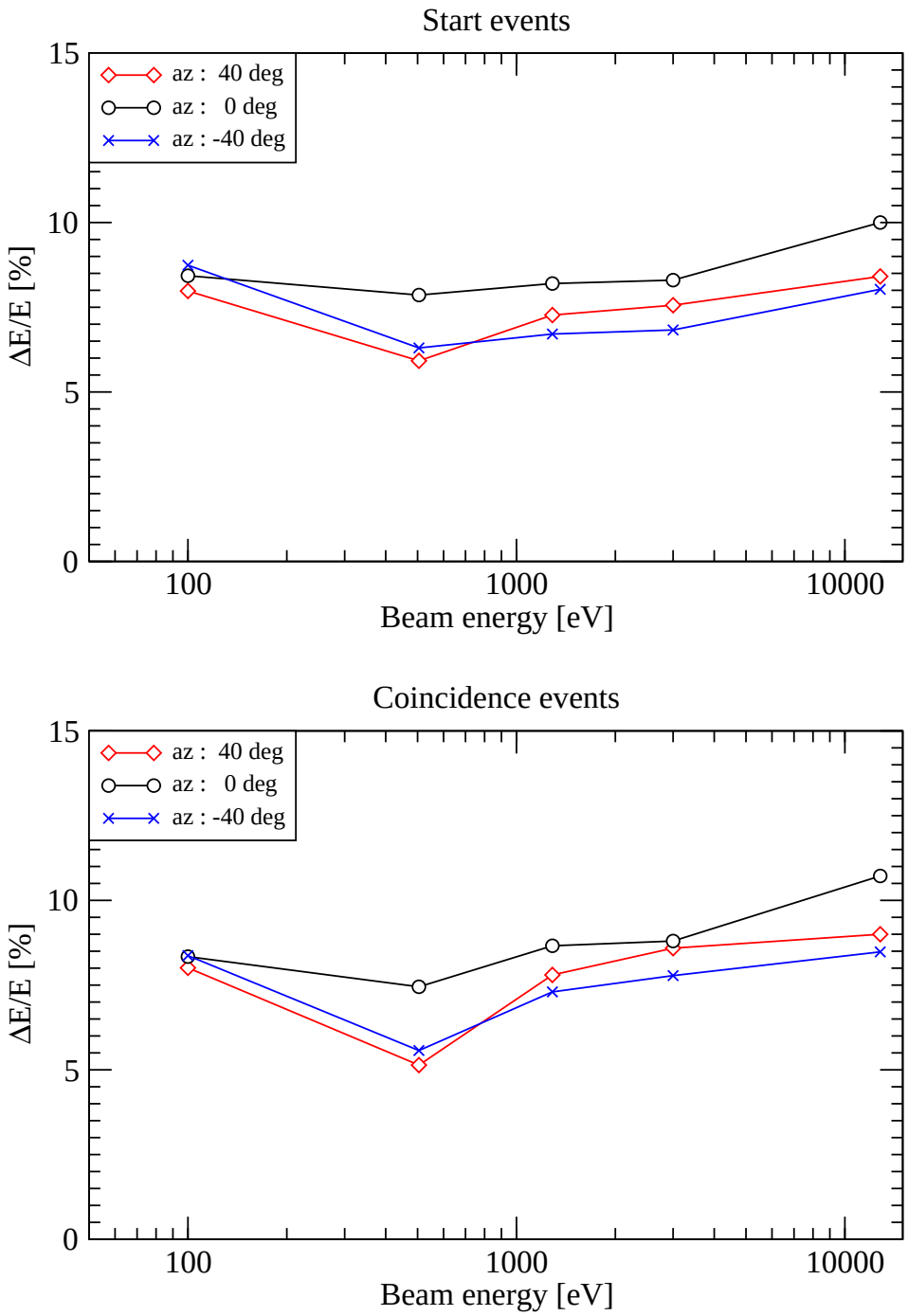

Figure 3.2: Energy resolution$\Delta E/E$. Top: using start counter data; bottom: using coincidence event data.

3.3 Energy sweep

The energy table used after commissioning is shown in Table 3.3. Due to the double anglular scan, two consecutive energy steps on the DPU have the same center energy but different viewing directions.

Table 3.3: Energy tables as used after commissioning. Angular ordered numbering is used. To convert to DPU numbering, see Equations 3.1 and 3.2.

Energy bin E	Energy bins e	Center energy [eV]
0	0,1	109
1	2,3	136
2	4,5	169
3	6.7	210
4	8,9	262
5	10,11	327
6	12,13	408
7	14,15	509
8	16,17	636
9	18,19	794
10	20,21	992
11	22,23	1,240
12	24,25	1,549
13	26,27	1,935
14	28,29	2,418
15	30,31	3,022

3.4 Angular pixels

The shape of angular pixels depends on viewing direction. The azimuth angle φ and elevation angle θ is used to describe the pixel shape. Looking direction with azimuth φ= -90° points to nadir, and φ =+90° points to zenith for nominal s/c attitude. See Figure 1.1 for the relation of these angles relative to the instrument coordinate system. Figure 3.3 shows the shape of an enter looking pixel at azimuth φ of approximately 0°. The shape does not depend much on weather start counters data or coincidence data is used. For calibration, 7 viewing directions (with approximate azimuth φ = -64°, -34°, -16°, 0°, 16°, 34°, 64°) were measured. Pixel shape was then parametrized to obtain the shape for arbitrary intermediate viewing directions.

Pixel shape as a function of the elevation direction θ is in first oder independent of the azimuthal viewing direction φ, i.e. independent of the pixel D, and is well approximated by a gaussian. Pixel shape as a function of the azimuthal direction φ changes pixel by pixel. The parametrization of the azimuthal shape using two free parameters, the azimuthal direction and energy normalized deflection function dVE, is employed here in analogy to the analyzer constant used for the electrostatic analyzer. Here dVE is defined by

$$dVE\left(\varphi_c\right) = \frac{\Delta U_{defl}\left(\varphi_c\right)}{E_{center}} \tag{3.5}$$

where φ_c denotes the azimuth angle in degrees of the center of the pixel (the *viewing direction*), $\Delta U_{defl} = U_{deflupper} - U_{defllower}$ the viewing direction dependent voltage difference required between the upper and lower deflector electrode in volts, and E_{center} the center energy selected by the ESA in eV. As the independent variable is actuallyφ_c, the required value of dVE (which in turn defines the voltages applied to the deflection system according to Equation 3.5) is obtained using an empirical fit function:

$$dVE\left(\varphi_c\right) = -0.5078 \cdot \sin\left[\left(0.9748 \cdot \varphi_c + 0.1016\right)\frac{\pi}{180°}\right] \tag{3.6}$$

The full pixel shape in elevation angle θ and azimuth angle φ is modelled by an asymetric 2D gauss function $Y(\theta, \varphi)$:

$$Y(\theta,\varphi) = max\left(0, A_4 + A_0 \cdot \begin{cases} (\varphi - A_1) > 0 & : \quad e^{-\left[\frac{(\varphi-A_1)^2}{2[A_2(1-A_3)]^2} + \frac{(\theta-B_1)^2}{2B_2^2}\right]} \\ else & : \quad e^{-\left[\frac{(\varphi-A_1)^2}{2[A_2(1+A_3)]^2} + \frac{(\theta-B_1)^2}{2B_2^2}\right]} \end{cases}\right) \tag{3.7}$$

with elevation angle θ and azimuth angle φ given in degrees, $max(a, b)$ returning the larger of the two values a and b, and A_n and B_n shape parameters.

A total of 7 angular pixels were characterized during calibration and pixel shapes were fitted using Equation 3.7. Shape parameters A_n and B_n from these measurements are shown in Figure 3.4. Empirical functions were used to fit these data to interpolate shape parameters for all 16 pixels from Table 3.1. The result of this process is shown in Tables 3.4 and 3.5, and the resulting pixel shapes are depicted in Figure 3.5.

Table 3.4: Summary of parameters A_n

Parametrization in azimutal direction φ						
Pixel name	dVE	Ampl. A0	Center A1	Sigma A2	Skew A3	Offset A4
CH-0L	0.43	0.12	-63.10	7.49	0.24	0
CH-1L	0.34	0.33	-46.04	5.74	0.13	0
CH-2L	0.21	0.63	-27.27	3.92	0.00	0
CH-3L	0.07	0.95	-9.74	2.87	-0.13	0
CH-4L	-0.07	0.80	7.09	2.77	-0.23	0
CH-5L	-0.21	0.56	24.62	3.62	-0.32	0
CH-6L	-0.34	0.34	43.40	5.27	-0.38	0
CH-7L	-0.44	0.17	62.84	7.09	-0.41	0
CH-0H	0.39	0.21	-54.78	6.66	0.19	0
CH-1H	0.27	0.49	-35.46	4.66	0.06	0
CH-2H	0.13	0.81	-17.08	3.20	-0.08	0
CH-3H	0.00	0.92	-1.32	2.70	-0.18	0
CH-4H	-0.13	0.69	14.43	3.02	-0.27	0
CH-5H	-0.27	0.46	32.81	4.28	-0.35	0
CH-6H	-0.39	0.25	52.13	6.12	-0.40	0
CH-7H	-0.45	0.15	65.41	7.30	-0.41	0

Table 3.5: Summary of parameters B_n

Parametrization in elevation direction θ		
Pixel	Center B1	Sigma B2
any	0.00	3.25

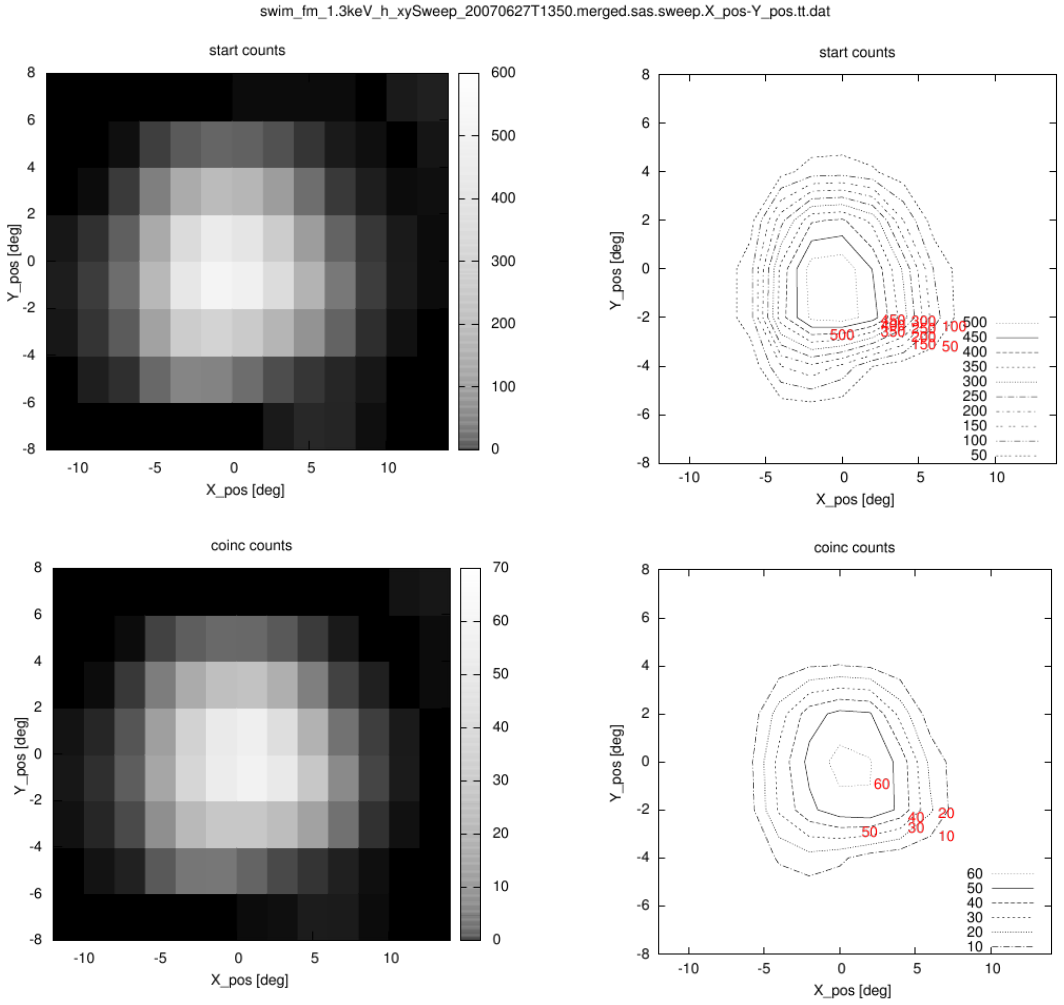

Figure 3.3: Example of angular pixel shape (using H^+,1300 eV). The pixel position corresponds most closely to pixel CH-3H from Table 3.1). X_pos denotes the azimuth angle in degrees. Y_pos the elevation angle in degrees. Intensity is normalized to an arbitrary scale, the ratio between the two plots is correct however. The shape of the top pannel is derieved from start events, the bottom pannel from coincidence events. Note the highly nonlinear color scale.

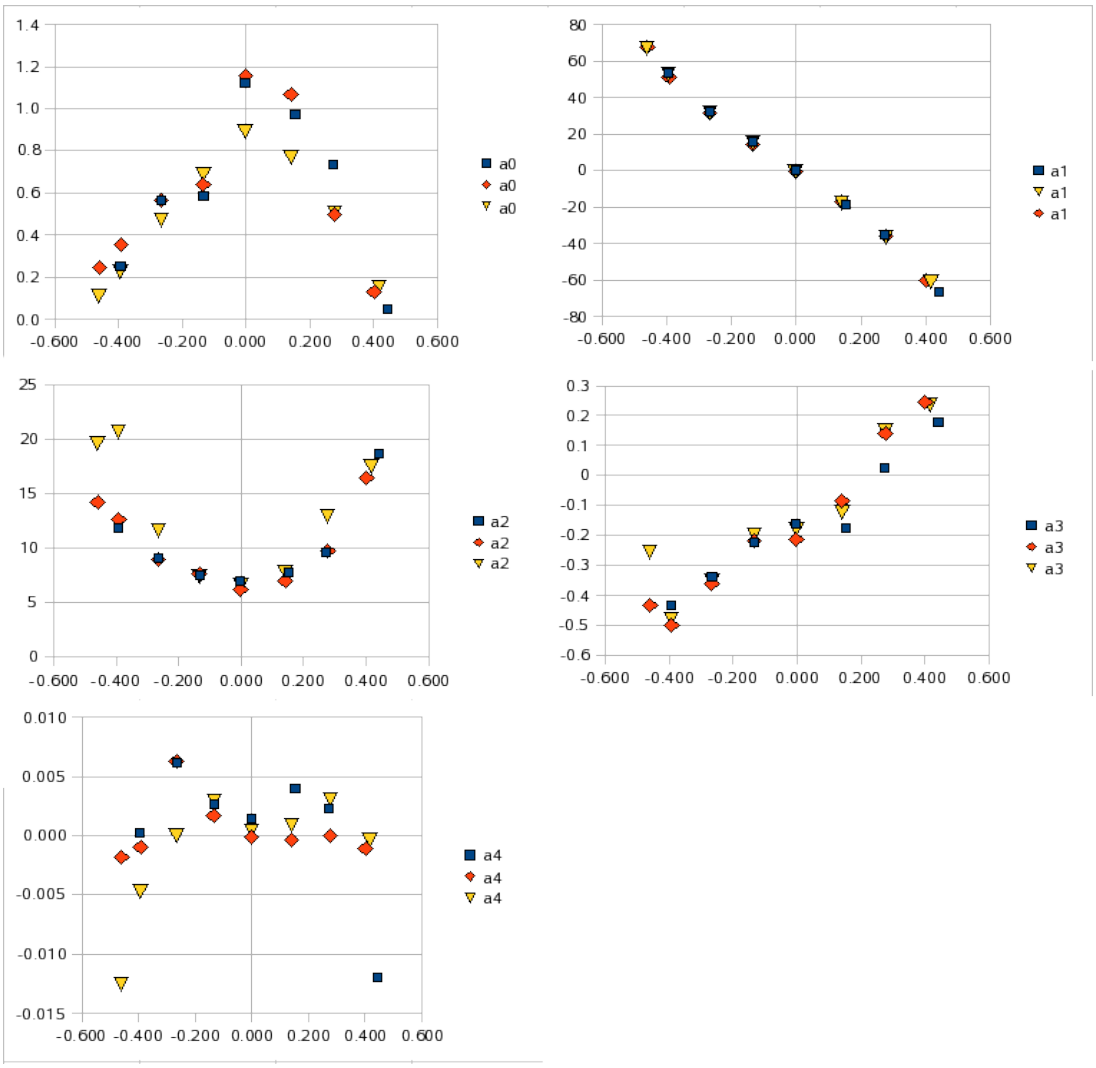

Figure 3.4: Collection of parameter sets An in equation 3.7 obtained from a fitting of measured pixel shapes. X-axis on all plots is dVE. The colors indicate three different datasets obtained independently.

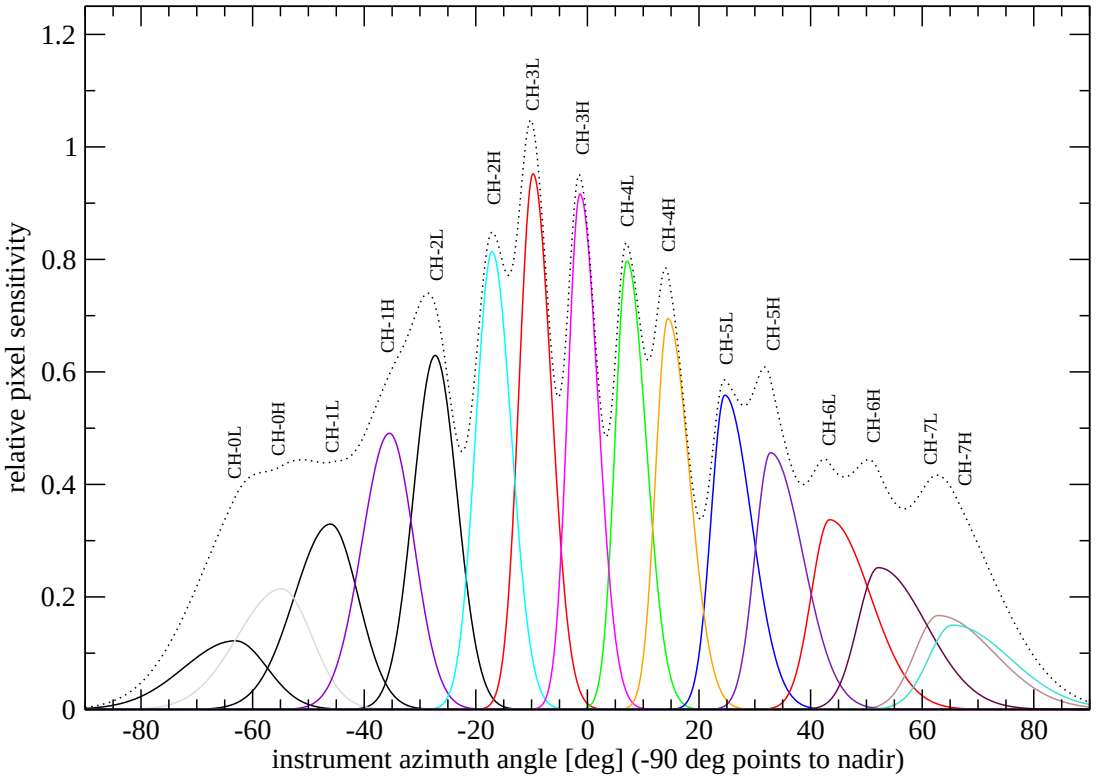

Figure 3.5: SWIM pixel shapes in azimutal direction for 16 pixels. The dotted line is the sum of the response function of all pixels. To obtain a flat response over azimuth, appropriate weighting of each pixel is needed.

3.5 Mass resolution

ToDo: Insert mass resolution data here...

3.6 Accumulation time

Accumulation time for one measurement cycle is 8 seconds. Multiples of 8 seconds are also possible in principle, but this was never used during the mission. The sensor changes energy and/or deflection settings every $t_{SLOT} = 31.25$ms. This results in 256 possible slots in a measurement cycle. However, the two last slots (No. 254 and No. 255) are used internally and the data obtained during these slots is always zero.

$$\Delta t = \frac{8s}{256} = t_{SLOT} = 31.25\text{ms} \tag{3.8}$$

3.7 Binning

3.7.1 Mass calculation and binning

Mass m/q of a particle is calculated onboard by evaluating

$$(1 - \eta\,(m, E_p)) \cdot [E_p + U_{TOF} \cdot e \cdot q] = \frac{1}{2} m\, m_p\, v^2 \tag{3.9}$$

where E_p is the energy of the particle, η the fraction of energy loss at the start surface depending on the particle mass and particle energy, U_{TOF} the post-acceleration which the particle experiences when reaching the TOF section, e the elementary charge, q the charge of the ion, m_p the proton mass, v the velocity of the particle in the TOF section, and m the mass in amu. The calculation does not include any energy losses at various reflecting surfaces for reasons given below. By using $v = \frac{s}{t}$, where s the path length in the TOF section and t the measured TOF, and $U_P = E_P/\,(e \cdot q)$, $\sqrt{m/q}$ can be obtained by

$$\sqrt{m/q} = k(U_P) \cdot t = \left[\sqrt{\frac{2e}{m_p}} \cdot \sqrt{(1 - \eta\,(m, E_p)) \cdot (U_{TOF} + U_P)\, e} \cdot s^{-1} \right] \cdot t \tag{3.10}$$

The factor $k(U_P)$ is tabulated in the ETOF table onboard. The energy loss $\eta\,(m)$ at the start surface is difficult to know exactly. The tabulated value in the ETOF table therfore assumes $\eta\,(m, E) = 0$ for all m and E. This results in a overestimation of $\sqrt{m/q}$ for large values of m/q, but removes cumbersome energy and mass dependency of η form the lookup tables. Table 3.6 shows the parameters used to characterize the TOF cell.

Table 3.6: TOF section properties used to calculate onboard lookup tables

Parameter	Value
Energy loss, η	0%
TOF cell length, s	30 mm

The mass bin number M is calculated by mapping $\sqrt{m/q}$ from Equation 3.10 to 32 mass bins, numbered from 0 to 31:

$$M = \min \left[\text{floor} \left(\frac{\sqrt{m/q}}{\sqrt{m_{max}}} \cdot 32 \right), 31 \right] \tag{3.11}$$

$\min(a, b)$ returns the smaller of two values, $floor(x)$ rounds down to the lext lower integer number. $m_{max} = 64$. The min-function is to collect all $m/q > m_{max}$ in the highest mass bin $M = 31$. Table 3.7 shows the mass bins with assumption of no energy loss at the start surface .

Table 3.7: Ideal mass bin mapping table without energy loss on start surface. H^+will mostly show in mass bin 4 due to only small energy loss. Bin 31 is a "catch-all" bin for $m > 64$amu.

mass bin M	from [amu]	to [amu]
0	0.00	0.06
1	0.06	0.25
2	0.25	0.56
3	0.56	1.00
4	1.00	1.56
5	1.56	2.25
6	2.25	3.06
7	3.06	4.00
8	4.00	5.06
9	5.06	6.25
10	6.25	7.56
11	7.56	9.00
12	9.00	10.56
13	10.56	12.25
14	12.25	14.06
15	14.06	16.00
16	16.00	18.06
17	18.06	20.25
18	20.25	22.56
19	22.56	25.00
20	25.00	27.56
21	27.56	30.25
22	30.25	33.06
23	33.06	36.00
24	36.00	39.06
25	39.06	42.25
26	42.25	45.56
27	45.56	49.00
28	49.00	52.56
29	52.56	56.25
30	56.25	60.06
31	60.06	inf

Note that current flight tables are calculated using an analyzer constant k of 4.255. The current best value for k is 4.250 (see Equation 3.4).

3.7.2 TOF peak shapes

ToDo: Add plots and fit functions for TOF-peak shapes for various m/q here...

3.7.3 Mass scale including energy loss

ToDo: Add definitions for mass scale with energy loss here...

3.8 Geometric factor

In the following text, i denotes the energy step, n angular pixel and m the ion species (this is not the mass bin number M, as one species can cover more than one mass bin). The angular ordered pixel numbering is used throughout this section. For easier understanding, a corresponding units of the values are shown in parenthesis []. The differential number flux $J_{n,i,m}$ [#/(sr cm^2 eV s)] seen by each pixel n and energy step i with a energy width of ΔE_i [eV], and species m is given by

$$J_{n,i,m} = \frac{C_{n,i,m}}{\widetilde{G}^m_{n,i} \cdot \Delta E_i \cdot \Delta t} \tag{3.12}$$

with $C_{n,j,m}$ [#] the number of counts accumulated during the duty cycle Δt [s], and $\widetilde{G}^m_{n,i}$ is the mechanical geometric factor [cm^2 sr] including all the efficiencies. The duty cycle for SWIM sensor is 1/32 s. The combined geometric factor $\widetilde{G}^m_{n,i} \cdot \Delta E_i$ [cm^2 sr eV] for each pixel n at the energy step i is approximated as

$$\widetilde{G}^m_{n,i} \cdot \Delta E_i = k_{n,i,m} \cdot A_n \cdot \Delta\Omega_n \cdot \left(\frac{\Delta E_i}{E_i}\right) \cdot E_i \tag{3.13}$$

with $\Delta E_i/E_i$ the energy resolution of the electrostatic analyzer, E_i the center energy of energy bin of i, $k_{n,i,m}$ representing all the efficiencies, A_n the open area, $\Delta\Omega_n$ the angular pixel size. Using

$$G^m_{n,i} = k_{n,i,m} \cdot A_n \cdot \Delta\Omega_n \cdot \left(\frac{\Delta E_i}{E_i}\right) \tag{3.14}$$

Equation 3.15 can be rewritten as

$$J_{n,i,m} = \frac{C_{n,i,m}}{G^m_{n,i} \cdot E_i \cdot \Delta t} \tag{3.15}$$

We factorize the geometrtic factor of individual pixel further using

$$G^m_{n,i} = g^{Start}_n \cdot \epsilon \cdot G_0(E_i, m) \tag{3.16}$$

by introducing g^{Start}_n, the geometric factor of pixel n relative to the reference geometric factor $G_0(E_i, m)$ and ϵ an efficiency factor depending on counter type used ($\epsilon = 1$ for start rate). This split was done because the ratios of the geometric factor between different pixels can be determined with much higher accuracy than the absolute value. $G_0(E_i, m)$ is by definition calculated using the start rate. For stop- or coincidence rates ϵ must be adjusted accordingly. To get $G^m_{n,i}$ values in Equation 3.15 from Equation 3.16, the tabulated values for $G_0(E_i, m)$ must be interpolated for each energy step center E_i.

Another way of looking at individual pixels is derived from 3.14 and using the pixel shape in Table 3.4. The pixel dependent factor g^{Start}_n is calculated from the pixel shape

$$g^{Start}_n = \frac{\iint Y_n(\theta, \varphi) d\theta d\varphi}{\iint Y_{CH-3L}(\theta, \varphi) d\theta d\varphi} \tag{3.17}$$

3.8.1 Geometric factor for hydrogen

The relative geometric factor g^{Start}_n normalized to the reference pixel of CH-3L using the 1300eV H^+ beam for the start counter is shown in Figure 3.6 and Table3.8. The tabulated values are valid for the energy range of 500 eV .. 3000 eV. The values in Table 3.8 does not yet include the slightly higher energy resolution at large deflection angles φ. This leads to a slight overestimation (~10%) of the relative geometric factor for pixels with $|\varphi| > 40°$. The absolute geometric factor $G_0(E_i, H^+)$ for the reference pixel of CH-3L used for normalization depends slightly on energy, with a higher value at lower energies (Table 3.9) . Use Equation 3.16 and values in Table 3.8 to get absolute geometric factors for each pixel for start events.

For coincidence rates, ϵ from Equation 3.16 becomes <1. For 1300eV H^+, the value obtained is shown in Equation 3.18, C_{coinc} and C_{start} denoting observed coincidence and start rates. It is important to verify this relation with flight data to get more accuracy.

$$\epsilon = \frac{C_{coinc}}{C_{start}} \simeq 0.11 \tag{3.18}$$

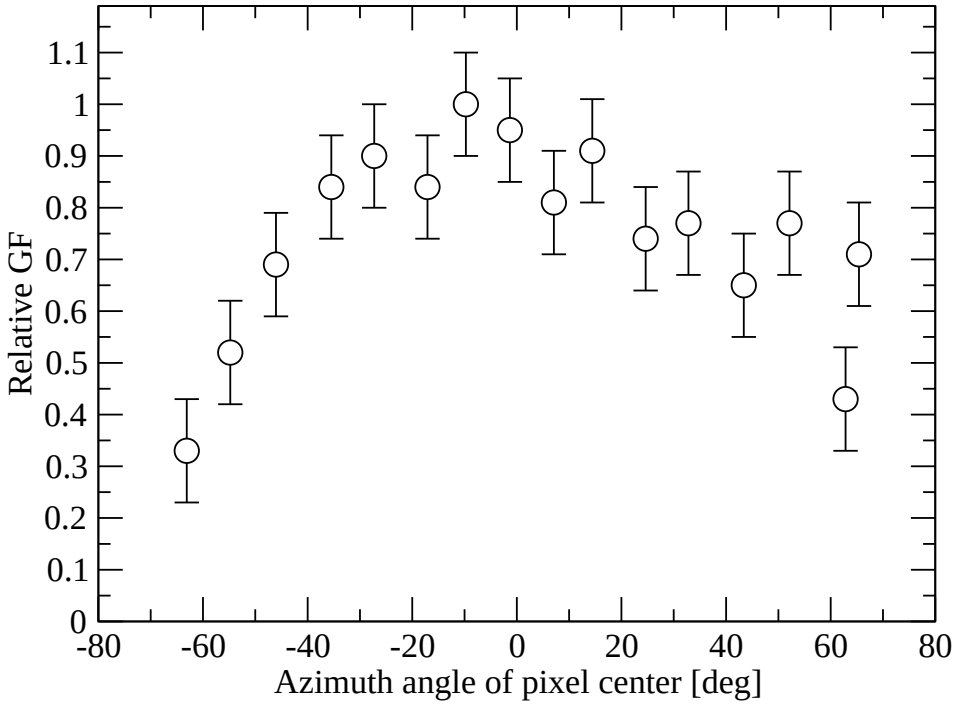

Figure 3.6: Relative geometric factor g_n^{Start} for H^+at 1300 eV versus pixel center direction

Table 3.8: Relative geometric factors g_n^{Start} for start counter and coincidence events for H^+. The values shown are strictly valid only for 500 eV .. 3000 eV H^+ only, but may be used for a larger energy range at the extent of an additional error.

Pixel name	relative GF g_n^{Start} for start counter (1σ)
CH-0L	0.33±0.1
CH-1L	0.69±0.1
CH-2L	0.90±0.1
CH-3L	1.00±0.1
CH-4L	0.81±0.1
CH-5L	0.74±0.1
CH-6L	0.65±0.1
CH-7L	0.43±0.1
CH-0H	0.52±0.1
CH-1H	0.84±0.1
CH-2H	0.84±0.1
CH-3H	0.95±0.1
CH-4H	0.91±0.1
CH-5H	0.77±0.1
CH-6H	0.77±0.1
CH-7H	0.71±0.1

Energy E [eV]	$G_0(E, H^+)$ [$\mathrm{cm^2\,sr\,eV/eV}$]
500	$5.54{\cdot}10^{-5}\left(\begin{smallmatrix}+100\%\\-50\%\end{smallmatrix}\right)$
1300	$5.37{\cdot}10^{-5}\left(\begin{smallmatrix}+100\%\\-50\%\end{smallmatrix}\right)$
3000	$4.29{\cdot}10^{-5}\left(\begin{smallmatrix}+100\%\\-50\%\end{smallmatrix}\right)$

Table 3.9: Absolute geometric factors G_0 for H^+. The errors given are a preliminary estimate.

Abbreviations

CENA Chandrayaan-1 Energetic Neutrals Analyzer

DPU Digital Processing Unit

ESA Electrostatic Analyzer

HV High Voltage

MCP Micro Channel Plate

SICD Software Interface Control Document

SWIM Solar Wind Monitor

TCTM Telecommand/Telemetry (Control Document)

TOF Time-Of-Flight